

Optimal Feature Transport for Cross-View Image Geo-Localization

Yujiao Shi¹, Xin Yu^{1,2}, Liu Liu¹, Tong Zhang¹, and Hongdong Li^{1,2}

¹Australian National University, Canberra, Australia.

{yujiao.shi, xin.yu, liu.liu, tong.zhang, hongdong.li}@anu.edu.au

²Australian Centre for Robotic Vision, Australia.

Abstract

This paper addresses the problem of cross-view image based localization, where the geographic location of a ground-level street-view query image is estimated by matching it against a large scale aerial map (e.g. a high-resolution satellite image). State-of-the-art deep-learning based methods tackle this problem as deep metric learning which aims to learn global feature representations of the scene seen by the two different views. Despite promising results are obtained by such deep metric learning methods, they, however, fail to exploit a crucial cue relevant for localization, namely, the spatial layout of local features. Moreover, little attention is paid to the obvious domain gap (between aerial view and ground view) in the context of cross-view localization. This paper proposes a novel Cross-View Feature Transport (CVFT) technique to explicitly establish cross-view domain transfer that facilitates feature alignment between ground and aerial images. Specifically, we implement the CVFT as a network layer, which transports features from one domain to the other, leading to more meaningful feature similarity comparison. Our model is differentiable and can be learned end-to-end. Experiments on large-scale datasets have demonstrated that our method has remarkably boosted the state-of-the-art cross-view localization performance, e.g., on the CVUSA dataset, with significant improvements for top-1 recall from 40.79% to 61.43%, and for top-10 from 76.36% to 90.49%, compared with the previous state of the art [14]. We expect the key insight of the paper (i.e. explicitly handling domain difference via domain transport) will prove to be useful for other similar problems in computer vision as well.

1. Introduction

This paper studies the problem of ground-to-aerial cross-view image-based localization. The task is: given a ground-

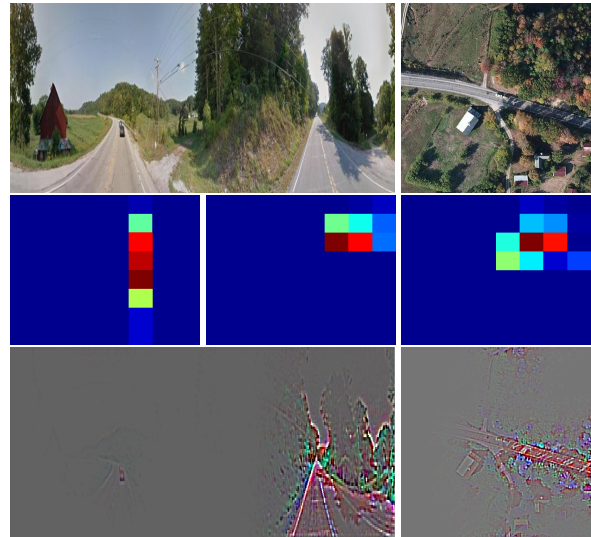


Figure 1: Illustration of the proposed Cross-View Feature Transport (CVFT). (a) First row: a panoramic ground-level query image (left), and its corresponding aerial image (right); (b) Second row: left: an example feature map learned from the ground image shown above; middle: the learned feature map from the aerial image shown above; Right: the transported ground-level feature map using our CVFT. It is clear that CVFT effectively aligns the two feature domains, bringing the two corresponding feature maps closer in the feature space; (c) Bottom row: visualizing the two feature maps [28].

level image of street scene (e.g. a Google street view image), we want to estimate where this image was taken, in terms of estimating its geo-location relative to a large (and geo-tagged) satellite map covering the region of interest (e.g. an entire city). Such a cross-view localization problem is not only practically relevant, thanks to the wide-accessibility of high-resolution satellite imagery, but also scientifically important and challenging. The challenges mainly come from the significant differences in their dif-

ferent viewpoints (one is from overhead, and the other at ground level) and vast variations in visual appearance.

Traditional methods for solving this problem are often based on image retrieval technique, namely, searching through the entire satellite map to find a particular local region (on the map) that is most similar to the given ground-level query image. Benefited from recent advance of deep learning, most state-of-the-art cross-view localization methods [7, 14, 29] treat this task as a deep metric learning problem. Specifically, they employ two-branch structured CNNs to extract deep features, which are then used to compare cross-view image pairs.

Despite many of the existing methods obtained decent results, their performance is limited by a few key oversights: (1) Their learned deep feature embeddings are often a global holistic scene representation, obtained via a global aggregation layer (*e.g.* global pooling or VLAD-type [9]), in which process very useful spatial feature layout information is lost. Such spatial layout information, however, is very useful for localization and is an important visual cue even for human self-localization. For example, when one is disorientated in a foreign city without any localization device except for a map, knowing certain types of features (*i.e.*, buildings, roads and trees) are visible from certain viewing directions is a very informative piece of information allowing them to re-oriented. Most state-of-the-art cross-view localization methods failed to exploit such information. (2) Although a multi-layer network is theoretically able to achieve such a forceful embedding, neglecting the image domain differences would lead to inferior results. For instance, the topology of ground images is cylinder (for a 360 panorama) while the topology of satellite images is disk. How to fully exploit this domain information for learning a better feature embedding remains unknown.

In this paper, we propose an effective mechanism to explicitly take into account both issues: (1) preserving local feature spatial layout information, and (2) implement a mechanism to account for feature domain differences. We first employ a two-branch Siamese-like CNN architecture to extract features from ground and aerial images separately. As seen in Figure 1, there is a spatial domain correspondence between ground panorama and aerial images. In order to exploit the spatial information of local features, we propose a Cross-View Feature Transport (CVFT) model to explicitly transform feature maps from one domain (ground) to the other one (aerial).

Specifically, we re-arrange feature maps extracted from one branch by a transport matrix. Then the transformed features from one domain will lie much closer to the corresponding features in the other domain in terms of positions, and facilitate similarity comparisons. Moreover, since the spatial layout information is also embedded into the features, our features are more discriminative.

Our transport matrix is estimated by a Sinkhorn layer, where differentiable Sinkhorn iterations are applied to optimize a doubly stochastic matrix. Since all the layers in our network can be differentiable, our CVFT model can be trained in an end-to-end fashion. Extensive experimental results demonstrate that our CVFT improves cross-view geo-localization performance by a large margin on standard benchmarks.

The contributions of this work are as follows:

- A Cross-View Feature Transport (CVFT) model for domain spatial transfer. Our CVFT model explicitly establishes feature transformations between two different domains, facilitating cross-domain feature similarity matching.
- A new state-of-the-art cross-view image based geo-localization method, which outperforms all previous best performing deep networks developed for this task.

2. Related works

Estimating the geographical location of a query ground image can be regarded as a image matching or retrieval task. Since the performance of existing methods highly rely on the image features, we classify them into two categories: hand-crafted feature based and deep feature based approaches.

Hand-crafted feature based approaches: In the past decades, traditional hand-crafted features are widely used for the image matching and retrieval tasks [2, 13, 18, 15]. However, it is very difficult to directly match local features between ground-view and aerial-view images since hand-crafted features cannot handle large viewpoint changes well. Thus, several methods [2, 13, 18] transform ground images to the bird-view images and then match the warped images to the aerial ones. Sivic and Zisserman [23, 24] aggregated a set of local features into a histogram of visual words, known as Bag of words, to obtain a global descriptor. They showed that the aggregated descriptors were partially viewpoint and occlusion invariant, and outperformed local feature matching. Later, Nister and Stewenius [19] involved more visual words by applying a tree structure vocabulary. Jegou *et al.* [9] aggregated the residuals of the local features to cluster centroids to represent an image, dubbed VLAD descriptors. However, due to the large geometric and appearance variations between the ground and aerial images, hand-crafted feature matching becomes the bottleneck of the performance of cross-view geo-localization.

Deep feature based approaches: Deep neural networks have proven their powerful ability on image representation [20]. The seminal work [26] attempted to introduce deep features to the cross-view matching task. Workman and Jacobs [26] fine-tuned AlexNet [12] on Imagenet [20] and Places [30]. Then, the deep network was employed to

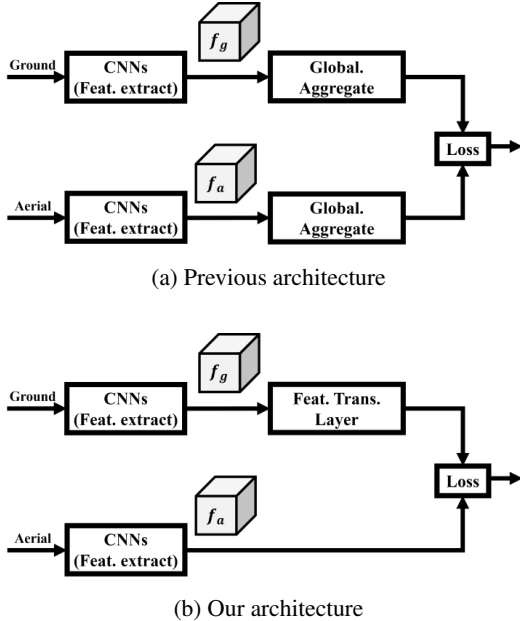


Figure 2: Comparison between traditional methods and ours. (a) Existing deep metric learning network with a global feature aggregation layer; (b) Our new network with a Feature Transport Layer. Global Feature Aggregation tends to discard very useful spatial layout information. In contrast, our Feature Transport Layer maps feature from the ground-view domain to the aerial domain, accounting for their domain difference. Details of the Feature Transport Layer will be explained in the main text.

extract features for cross-view matching/localization. The work [26] also demonstrates the superior discriminativeness of deep features in comparison to hand-crafted features. Workman *et al.* [27] further indicated that fine-tuning CNNs by minimizing the distance between aerial and ground-view images leads to better localization performance. Vo and Hays [25] proposed a set of CNN architectures (Classification, Hybrid, Siamese and Triplet CNN) for matching cross-view images. They achieved significant improvement on the retrieval accuracy by using a triplet CNN. Inspired by the success of NetVLAD in the place recognition task [1], Hu *et al.* [7] embed a NetVLAD layer on top of a VGG network to extract descriptors that are invariant against large viewpoint changes. However, their method lost spatial information of deep features. Liu *et al.* [14] found that orientations plays an important role in order to achieve more discriminative features. They incorporated per-pixel orientation information into a CNN to learn orientation-selective features for cross-view localization.

3. Motivation: Cross-View Feature Transport

Existing deep learning based Cross-View Localization methods often adopt a forced feature embedding procedure

that brings matchable ground-to-aerial image pairs closer in the feature embedding space while far apart for those non-matchable ones. In their implementations, a Global Aggregation operation (such as ‘global pooling’ or VLAD-type feature aggregation [1]) is often adopted.

However, these global aggregation steps often discard (or destroy) the spatial layout information of local deep features (in other words, the relative positions between those local features in the image plane). This spatial layout information is however very useful and plays a pivotal role in aiding human’s geo-localization (*e.g.* re-orientation or way-finding). For example, human usually memorize the relative spatial position of a certain object or building in a scene for the localization and navigation purpose.

To exploit such cues, we propose a novel feature transport block (in the form of differentiable neural layers) in this work, which is able to transport (transform or map) features from one domain (*e.g.* ground) to another (*e.g.* aerial). Fig. 2 shows a comparison between the traditional method using global feature aggregation, and our new method with a Feature Transport module.

Due to the obvious domain differences between a ground-view image and a satellite image (namely, the former is a panoramic image seen from the ground-level, while the latter depicts an overhead (bird-eye’s) view of a geographic region), simply computing the distance between two deep-features from different domains may neglect the important domain correspondences, thus yielding very biased estimation.

In this paper, we take a direct (and explicit) approach to tackle this issue to account for the domain gap, such as drastic appearance changes as well as geometric distortions. Inspired by the idea of Optimal transport (OT), we aim to resort a transport matrix (parameterized as a permutation matrix \mathbf{P}) to achieve this goal. To make the objective function can be optimized by a deep neural network, we relax all permutations as doubly Stochastic matrices, and implement the doubly-stochastic normalization procedure (known as Sinkhorn iteration) as a differentiable layer.

As long as an optimal transport map is learned, we can use it to transport a ground-view feature map to its corresponding location on the feature map of the aerial image, such that their feature domains can be spatially aligned. In the next section, we will give more technical details of the process.

3.1. Optimal Feature Transport

Optimal Transport (OT) theory was originally developed for finding the optimal transportation plan \mathbf{P}^* that can best align two probability distributions μ_s and μ_g . This is done by minimizing the following transport distance: $\langle \mathbf{P}, \mathbf{C} \rangle_F$, where $\langle \cdot, \cdot \rangle_F$ is the Frobenius norm between two matrices. $\mathbf{C} \in \mathcal{R}^{n_s \times n_t}$ is a cost matrix measuring cost for transport-

ing from source samples and the target samples, and \mathcal{P} is a set of transport plans and $\mathbf{P} \in \mathcal{R}^{n_s \times n_t}$. n_s is the number of source samples \mathbf{x}^s and n_t is the number of target samples \mathbf{x}^t .

Since solving OT is non-differentiable, training a deep neural network using OT raises formidable computational challenges. Thus, we employ an entropy-regularized optimal transport formulation [3, 6] in our framework. Specifically, given an aerial image \mathbf{A} , a ground image \mathbf{G} , the optimal transport matrix \mathbf{P}^* between \mathbf{A} and \mathbf{G} can be defined as:

$$\mathbf{P}^* = \arg \min_{\mathbf{P} \in \mathcal{P}} \langle \mathbf{P}, \mathbf{C} \rangle_F - \lambda h(\mathbf{P}), \quad (1)$$

where $h(\mathbf{P})$ is an entropy regularization term of \mathbf{P} and λ is a trade-off weight. The entropy regularization term forces the solution of Equation (1) to be smoother as λ increases, and sparser as λ decreases. \mathbf{P}^* is a doubly stochastic matrix.

After obtaining \mathbf{P}^* , we can transport the feature maps between the ground-view and aerial-view images as follows:

$$\mathbf{f}^i(a) = n_a \mathbf{P}^* \mathbf{f}^i(g), \quad \mathbf{f}^i(g) = n_g \mathbf{P}^{*T} \mathbf{f}^i(a), \quad i = 1, \dots, c, \quad (2)$$

where $\mathbf{f}^i(g) \in \mathcal{R}^{h \times w}$ and $\mathbf{f}^i(a) \in \mathcal{R}^{h \times w}$ represent the i -th channel CNN-extracted feature maps of the ground and aerial images, respectively; n_a and n_g represent the feature numbers of aerial and ground images in each channel, respectively. Here, the feature maps of ground and aerial images are extracted by deep neural networks, and h , w and c indicate the height, width and channel number of feature maps¹. Note that, in practice we only transport the ground-view feature domain to the aerial feature domain for sake of efficiency.

4. The Proposed Cross-View Geo-localization Networks

4.1. Network Architecture

Figure 3 illustrates the overview of our proposed CVFT framework. We first employ a two-branch Siamese-like architecture to learn feature maps for the ground and aerial images separately. In order to align the ground-view features to aerial-view features, we then exploit the idea of optimal transport to formulate the feature alignment. To be specific, we design a cost generation sub-network to generate a cost matrix for a ground image and a Sinkhorn layer is to optimize a feature transport matrix. Then, the feature transport matrix is applied to the ground-view feature maps. In this way, we re-arrange the spatial layouts of the ground-view feature maps and thus align them to their corresponding aerial ones. Finally, an objective function is employed to optimize our neural network in an end-to-end fashion.

¹The CNN-extracted ground feature map is resized to be the same as the aerial feature before feeding into the feature transport module.

4.2. Feature Extraction

Due to the powerful feature representation ability of deep convolutional neural networks, we employ a CNN, such as VGG [22], as our backbone network to extract features from input images. Since our backbone CNN, VGG network, outputs the feature maps with a high dimension, we apply another convolutional layer to reduce the feature dimension along the channel dimension rather than the spatial dimension. In this manner, we can preserve the spatial layout information of the extracted features.

4.3. Cost Matrix Generation

Ideally, we should use both the ground and aerial images to compute the cost matrix \mathbf{C} . However, it is very computationally expensive to calculate the cost matrix for each gallery image in large-scale retrieval problems. To speed up the efficiency of calculating \mathbf{C} , we only use one image from one domain to learn how to transform to the other domain. The other domain information is learned from the final objective function and the cost-matrix generation network is updated through backpropagation. As seen in Figure 3, we employ a regression layer to generate a cost matrix \mathbf{C} .

4.4. Sinkhorn Layer

Note that our cost matrix generation sub-network can easily generate a cost matrix with all positive elements, but it cannot directly generate a permutation matrix for the feature alignment because the generated matrix needs to be a doubly stochastic matrix [17, 21]. Therefore, we incorporate another layer, named Sinkhorn layer, to estimate a permutation matrix (*i.e.*, our feature transport matrix) from our generated cost matrix. The Sinkhorn layer implements the Sinkhorn algorithm [11, 4] to solve the entropy regularized optimal transport problem. Since Equation 1 is a strongly convex problem and the Sinkhorn iterations are differentiable, it can be solved efficiently by the Sinkhorn layer.

Specifically, given the cost matrix \mathbf{C} , the Sinkhorn algorithm first applies an exponential kernel on \mathbf{C} , yielding $\mathbf{C}' = \exp(-\lambda \mathbf{C})$. Second, the Sinkhorn algorithm normalizes rows and columns iteratively in order to convert \mathbf{C}' to a doubly stochastic matrix. Denote row $\mathcal{N}^r(\cdot)$ and column $\mathcal{N}^c(\cdot)$ normalization as follows:

$$\mathcal{N}_{i,j}^r(\mathbf{C}) = \frac{c_{i,j}}{\sum_{k=1}^N c_{i,k}}, \quad \mathcal{N}_{i,j}^c(\mathbf{C}) = \frac{c_{i,j}}{\sum_{k=1}^N c_{k,j}}, \quad (3)$$

where $c_{i,j}$ represents an element in \mathbf{C} . For the m -th iteration, the output of Sinkhorn operation $\mathcal{S}(\cdot)$ can be represented in a recursively manner:

$$\mathbf{P}^* = \mathcal{S}(\mathbf{C}) = \begin{cases} \mathbf{C} & m = 0, \\ \mathcal{N}^c(\mathcal{N}^r(\mathbf{C})) & \text{otherwise.} \end{cases} \quad (4)$$

When iterations converge, we thus obtain our feature transport permutation matrix.

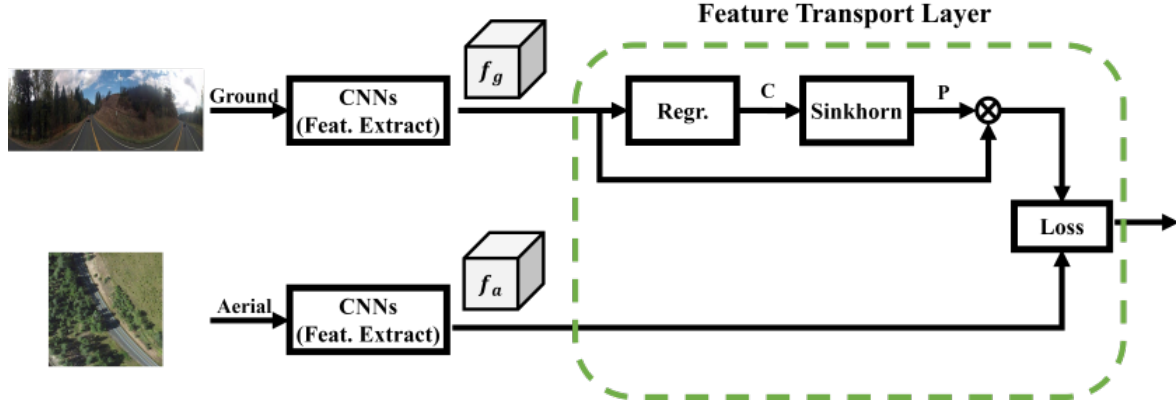


Figure 3: The framework of our method. A series of convolutional layers are applied to function as feature extractors, and then the extracted features are fed into a feature transport module to construct the correspondence between ground and aerial domains.

Note that, there are only linear operations in the Sinkhorn iterations, and thus the Sinkhorn layer is differentiable. We calculate the gradient with respect to the input by unrolling the sequence of the row and column normalization operations:

$$\frac{\partial \mathcal{S}}{\partial c_{s,t}} = \sum_{j=1}^N \frac{\partial \mathcal{S}}{\partial p_{s,j}} \left[\frac{[j=t]_{\mathbb{I}}}{\sum_{k=1}^N c_{s,k}} - \frac{c_{s,j}}{(\sum_{k=1}^N c_{s,k})^2} \right]. \quad (5)$$

where \mathcal{S} denotes the output of the Sinkhorn layer, $[\cdot]_{\mathbb{I}}$ represents an indication function, and s, t and j represent the indices of the row and columns in \mathbf{C} .

4.5. Triplet Loss on transported features

After transporting our ground-view feature maps, the ground-view features will be aligned to the aerial-view features. Then, we apply a metric learning objective to learn feature embedding for both the aligned ground-view images as well as aerial-view images. The triplet loss is widely used as an objective function to train deep neural networks for image localization and matching tasks [7, 14, 25]. The goal of the triplet loss is to bring matching pairs closer while pushing non-matching pairs far apart. Therefore, we employ a weighted soft-margin triplet loss as our objective to train our neural network, expressed as:

$$\begin{aligned} Loss &= \log(1 + \exp(\gamma(d_{pos} - d_{neg}))), \\ d_{pos} &= \sum_{i=1}^c \|\mathbf{P}^* \mathbf{f}^i(g) - \mathbf{f}^i(a^+)\|_2^2, \\ d_{neg} &= \sum_{i=1}^c \|\mathbf{P}^* \mathbf{f}^i(g) - \mathbf{f}^i(a^-)\|_2^2. \end{aligned} \quad (6)$$

where $\mathbf{f}(g)$, $\mathbf{f}(a^+)$ and $\mathbf{f}(a^-)$ represent the extracted features of the ground image, its corresponding aerial image

and an unmatching aerial image, respectively. d_{pos} and d_{neg} are the ℓ_2 distance of matching and unmatching image pairs. γ is a parameter to control the convergence speed and the gradient of the loss [7].

5. Experiments

Training and Testing Datasets We conduct our experiments on two standard benchmark datasets, namely CVUSA [29] and CVACT [14], for evaluation and comparisons. These two datasets are both cross-view datasets, and each containing 35,532 ground-and-satellite image pairs for training. CVUSA provides 8,884 image pairs for testing and CVACT provides the same number of pairs for validation (denoted as CVACT_val). CVACT [14] also provides 92,802 cross-view image pairs with accurate Geotags to evaluate Geo-localization performance (denoted as CVACT_test). Figure 4 illustrates some sample pairs from these two datasets.

Implementation Details We employ VGG16 with pre-trained weights on ImageNet [5] as our backbone network to extract image features. The convolutional feature maps of the conv5_3 layer in VGG16 are extracted as our image deep features. Similar to the work [7, 14], we set γ to 10 for the weighted soft-margin triplet loss. Our network is trained using Adam optimizer [10] with a learning rate of 10^{-5} and batch size of $B_s = 12$. We exploit an exhaustive mini-batch strategy [25] to construct the maximum number of triplets within each batch. For instance, for each ground-view image, there is 1 positive satellite image and $B_s - 1$ negative satellite images, and we can construct $B_s(B_s - 1)$ triplets in total. Similarly, for each satellite image, there is 1 positive ground-view image and $B_s - 1$ negative ground-view images, and thus $B_s(B_s - 1)$ triplets can also be estab-



Figure 4: Samples of ground and aerial image pairs. Left are ground panorama images and rights are the aerial images. The first two pairs are from CVUSA dataset and the last two pairs are from CVACT dataset.

lished. Since we use ground-view images as query images and aerial images as gallery images, our training triplets are constructed by a matching pair of a ground image and an satellite image and a negative satellite image. The source code will be released soon.

Evaluation Metrics We apply the same evaluation metric as [7, 14, 25], known as Recall@K, to exam the performance of our method as well as compare with state-of-the-art cross-view localization methods. Recall@K measures the performance that how many satellite images in the database need to be retrieved to find the true matching image. More detailed explanations of Recall@K metric can be found in [7, 25].

5.1. Effects of Cross-view Feature Transport

In this part, we conduct an ablation study to demonstrate the effectiveness of our proposed Cross-View Feature Transport (CVFT) module and how much our CVFT contributes to improving the geo-localization performance.

Baseline Networks: To illustrate the effectiveness of our proposed CVFT module, we simply remove it in our framework while keeping all the other parts as our first baseline network, named Our network wo/ CVFT. Then we retrain this baseline network. In this case, we still preserve the relative spatial information of local features but do not explicitly construct the cross-view correspondences in learning the network. The performance of our first baseline network is shown in Table 1. The recalls for the top-1 candidate on CVUSA and CVACT_val datasets are 41.68% and 45.28%, respectively. In comparisons to our proposed network, we conclude that it is difficult for our first baseline network to establish such spatial correspondences or transportation, thus leading to inferior localization performance.

Furthermore, in order to demonstrate the importance of the feature spatial layout information, we employ another baseline network, called VGG global pooling. For this baseline network, we apply global max pooling to the feature maps extracted by the layer conv5_3 in VGG16 as our image representation. Then we retrain this baseline network. As seen in Table 1, the recall performance for our second baseline network is the worst. This phenomenon indicates that the feature spatial layout information plays a critical role in the cross-view geo-localization task.

Our Network with CVFT: Since our propose network not only explores the spatial layout information but also explicitly establishes the domain correspondences via our CVFT, our network achieves the best performance as indicated by Table 1. Figure 5 shows the complete performance in terms of recalls. As visible in Figure 5, the recall performance of our network is consistently better than our baselines, and our network outperforms the baseline networks by a large margin on both CVUSA and CVACT_val datasets. For example, we obtain over 15% improvements at recall@1 on both datasets with the help of our CVFT module.

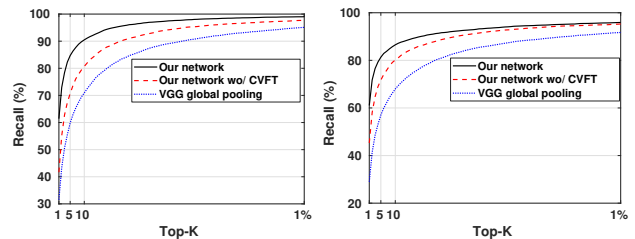


Figure 5: Comparison of Recalls on CVUSA (Left) and CVACT_val (Right) datasets. Our method outperforms baseline methods by a large margin, with a relative improvement of 19.75% and 15.77% at Top-1 for CVUSA and CVACT_val datasets, respectively.

5.2. Visualization of Cross-View Feature Alignment

The core insight of our method is that our CVFT is able to align the feature maps from a cross-view image pair. To verify this intuition, we show two examples of cross-view feature map alignments in Figure 7. As visible in Figure 7, we demonstrate two features from the ground-view images (the first column) as well as two features from the aerial-view images (the second column). After applying our estimated feature transport plan P^* to the ground-view features, we obtain transported ground features. Compared with the features directly extracted from the aerial images, our transported ground features are well aligned to them. This experiment not only shows the effectiveness of our CVFT but also demonstrates that our network can explicitly establish the relationship between the ground and aerial

Table 1: Recall performance on CVUSA [29] and CVACT_val dataset [14].

Method \ Dataset	CVUSA				CVACT_val			
	r@1	r@5	r@10	r@top 1%	r@1	r@5	r@10	r@top 1%
VGG global pooling	31.53	59.85	70.91	95.09	28.98	57.04	67.96	91.72
Our network wo/ CVFT	41.68	70.71	80.71	97.70	45.28	71.74	80.14	95.28
Our network	61.43	84.69	90.49	99.02	61.05	81.33	86.52	95.93

domains, thus facilitating our cross-view matching. Note that our permutation matrix \mathbf{P} is different from spatial transformer networks (STN) [8], since cross-view feature transformation cannot be modeled by geometric transformation of few parameters.

5.3. Comparisons with the State-of-the-Art

Retrieval on Cross-View Geo-localization We compare our method with the state-of-the-art cross-view localization methods, including Workman *et al.* [27], Vo *et al.* [25], Zhai *et al.* [29], CVM-net [7] and Liu *et al.* [14]. Following the previous works, we also report the recall at top 1% performance in Table 2. Since the recall@1% performance is also affected by the scale of the database, we thus report more challenging and practical evaluation results on recalls at top-1,5,10 in Table 3, and Figure 6 presents the complete Recall@K performance.

As indicated by Table 2, our method outperforms the state-of-the-art methods significantly. However, as the size of the database increases, the number of gallery images increases. Thus, using the retrieved results at recall at top 1% may be impractical. For instance, there would be more than 80 images in the retrieved results in CVUSA. Therefore, using recalls at top-1, 5, 10 would be more reasonable since the results can be easily analyzed by humans. Table 3 illustrates the performance of state-of-the-art methods on recalls at top-1, 5, 10. Compared to the state-of-the-art, our method outperforms the second best method [14] by a large margin. In particular, our network improves 20.64% and 14.09% on the recalls at top-1 for CVUSA and CVACT_val datasets, respectively. Table 3 also indicates our method is more practical for real-world cases.

Accurate Geo-localization We also conduct evaluation on the large-scale CVACT_test dataset [14] to show the effectiveness of our method for accurate city-scale Geo-localization applications. In addition, we also compare with the state-of-the-art methods, CVM-net [7] and Liu *et al.* [14], on this task.

In this experiment, we follow the evaluation protocol used in [1]. To be specific, a query image is deemed correctly geo-localized if at least one of the top K retrieved database satellite images is within the distance $d = 25m$ from the ground-truth position of the query image. The per-

Table 2: Comparison of recall @top 1% by state-of-the-art methods on CVUSA dataset [29].

	Workman [27]	Zhai [29]	Vo [25]	CVM-net [7]	Liu [14]	Ours
r@top 1%	34.30	43.20	63.70	93.62	96.12	99.02

centage of correctly localized queries (recall) is then plotted for different values of K , marked as recall@ K . The recall@ K performance is shown in Figure 8. As expected, our method still significantly outperforms the second-best method [14], with an improvement of 28.87% at top-1. We also show some localization examples in Figure 9 and 10, thus demonstrating the superiority of our method for localizing cross-view images in different scenarios.

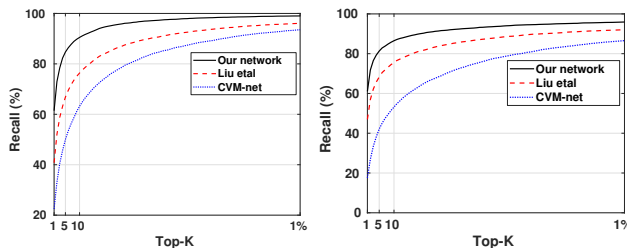


Figure 6: This figure shows that with our cross-view feature transport module, we outperform all state-of-the-art methods by a large-margin on CVUSA (Left) and CVACT_val (Right) datasets.

6. Conclusion

We have proposed a new cross-view image based geo-localization deep network in this paper. Our major contribution as well as the central innovation is the introducing of a novel cross-view feature transport layer (CVFT) which effectively bridges the gap between two different feature domains by transforming features from one domain to the other. In contrast to conventional approaches using deep metric learning to match corresponding feature pairs, our method provides a superior and more sensible solution. We believe the key idea of this paper (explicitly handling domain differences) is also valuable for solving many other problems in computer vision and machine learning. For the task of large-scale cross-view localization, our method has significantly improved performance in terms of top-K re-

Table 3: Comparison of recall performance with CVM-net [7] and Liu et al [14] on CVUSA [29] and CVACT_val [14]

Method \ Dataset	CVUSA				CVACT_val			
	r@1	r@5	r@10	r@top 1%	r@1	r@5	r@10	r@top 1%
Our network	61.43	84.69	90.49	99.02	61.05	81.33	86.52	95.93
Liu et al [14]	40.79	66.82	76.36	96.12	46.96	68.28	75.48	92.04
CVM-net [7]	22.47	49.98	63.18	93.62	17.53	42.13	53.15	86.72

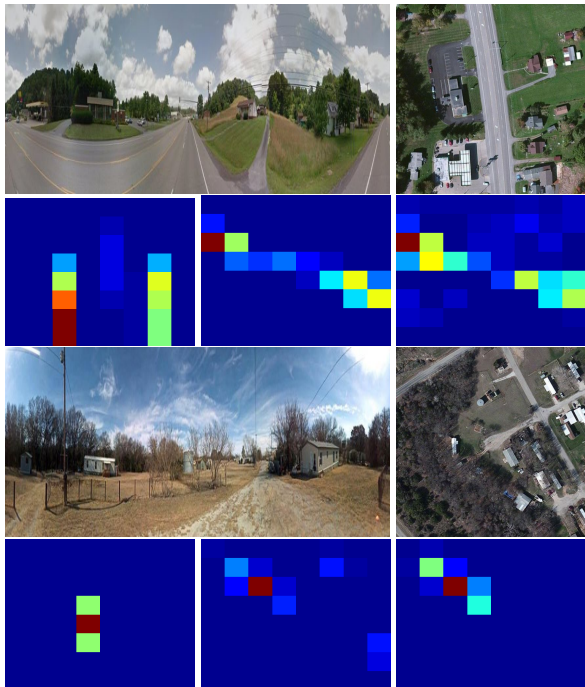


Figure 7: Our method successfully aligns cross-view feature maps by using CVFT feature transport. In each of the second rows: (Left column:) Input ground-view feature map; (Middle column) the corresponding satellite image feature map; (Right column) CVFT-transported ground feature map. Note the two feature maps are better aligned.

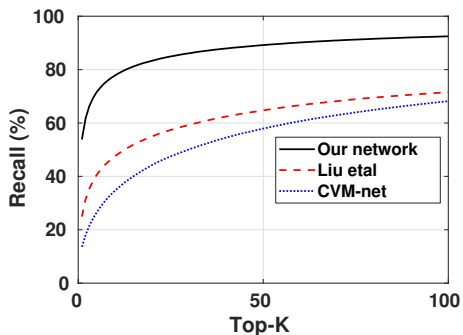
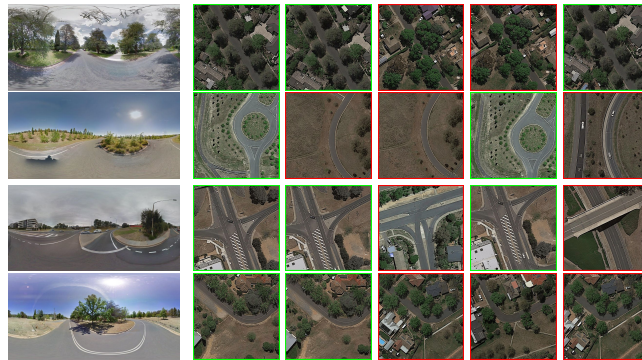


Figure 8: This graph shows that we achieve much higher localization performance (measured by recalls) than previous state-of-the-arts.



(a) Query (b) Top 1 (c) Top 2 (d) Top 3 (e) Top 4 (f) Top 5

Figure 9: Sample localization results by our method on ACT_test dataset. From left to right: ground-view query image and the Top 1-5 retrieved satellite images. Green and red borders indicate correct and incorrect retrieved results, respectively. Note that our method can localize versatile query images (e.g., suburbs and traffic intersection). (Best viewed in color on screen)



(a) Query (b) Top 1 (c) Top 2 (d) Top 3 (e) Top 4 (f) Top 5

Figure 10: Comparisons of different methods on ACT_test dataset. first row: top-5 recall results by our method; Second row: Liu *et al.* result [14]; third row: CVM-net [7]. Green and red borders indicate correct and incorrect retrieved results, respectively. Note that our method remains robust for this challenging scenario with many repetitive features.

call rate, demonstrating the power of our feature transport framework. Our method currently assumes the input query image is a full 360-degree panorama with known orientation, but we argue this restriction can be relaxed under the same theoretical framework of CVFT, and this is left as a possible future extension.

References

- [1] R. Arandjelovic, P. Gronat, A. Torii, T. Pajdla, and J. Sivic. Netvlad: Cnn architecture for weakly supervised place recognition. In *Proceedings of the IEEE Conference on Computer Vision and Pattern Recognition*, pages 5297–5307, 2016. [3](#), [7](#)
- [2] F. Castaldo, A. Zamir, R. Angst, F. Palmieri, and S. Savarese. Semantic cross-view matching. In *Proceedings of the IEEE International Conference on Computer Vision Workshops*, pages 9–17, 2015. [2](#)
- [3] N. Courty, R. Flamary, D. Tuia, and A. Rakotomamonjy. Optimal transport for domain adaptation. *IEEE transactions on pattern analysis and machine intelligence*, 39(9):1853–1865, 2017. [4](#)
- [4] M. Cuturi. Sinkhorn distances: Lightspeed computation of optimal transport. In *Advances in neural information processing systems*, pages 2292–2300, 2013. [4](#)
- [5] J. Deng, W. Dong, R. Socher, L.-J. Li, K. Li, and L. Fei-Fei. Imagenet: A large-scale hierarchical image database. In *2009 IEEE conference on computer vision and pattern recognition*, pages 248–255. Ieee, 2009. [5](#)
- [6] C. Frogner, C. Zhang, H. Mobahi, M. Araya, and T. A. Poggio. Learning with a wasserstein loss. In *Advances in Neural Information Processing Systems*, pages 2053–2061, 2015. [4](#)
- [7] S. Hu, M. Feng, R. M. H. Nguyen, and G. Hee Lee. Cvmnet: Cross-view matching network for image-based ground-to-aerial geo-localization. In *The IEEE Conference on Computer Vision and Pattern Recognition (CVPR)*, June 2018. [2](#), [3](#), [5](#), [6](#), [7](#), [8](#), [10](#)
- [8] M. Jaderberg, K. Simonyan, A. Zisserman, et al. Spatial transformer networks. In *Advances in neural information processing systems*, pages 2017–2025, 2015. [7](#)
- [9] H. Jégou, M. Douze, C. Schmid, and P. Pérez. Aggregating local descriptors into a compact image representation. In *Computer Vision and Pattern Recognition (CVPR), 2010 IEEE Conference on*, pages 3304–3311. IEEE, 2010. [2](#)
- [10] D. P. Kingma and J. Ba. Adam: A method for stochastic optimization. *arXiv preprint arXiv:1412.6980*, 2014. [5](#)
- [11] J. Kosowsky and A. L. Yuille. The invisible hand algorithm: Solving the assignment problem with statistical physics. *Neural networks*, 7(3):477–490, 1994. [4](#)
- [12] A. Krizhevsky, I. Sutskever, and G. E. Hinton. Imagenet classification with deep convolutional neural networks. In F. Pereira, C. J. C. Burges, L. Bottou, and K. Q. Weinberger, editors, *Advances in Neural Information Processing Systems 25*, pages 1097–1105. Curran Associates, Inc., 2012. [2](#)
- [13] T.-Y. Lin, S. Belongie, and J. Hays. Cross-view image geolocalization. In *Proceedings of the IEEE Conference on Computer Vision and Pattern Recognition*, pages 891–898, 2013. [2](#)
- [14] L. Liu and H. Li. Lending orientation to neural networks for cross-view geo-localization. In *The IEEE Conference on Computer Vision and Pattern Recognition (CVPR)*, June 2019. [1](#), [2](#), [3](#), [5](#), [6](#), [7](#), [8](#), [10](#), [12](#)
- [15] L. Liu, H. Li, and Y. Dai. Efficient global 2d-3d matching for camera localization in a large-scale 3d map. In *Proceedings of the IEEE International Conference on Computer Vision*, pages 2372–2381, 2017. [2](#)
- [16] L. v. d. Maaten and G. Hinton. Visualizing data using t-sne. *Journal of machine learning research*, 9(Nov):2579–2605, 2008. [10](#), [12](#)
- [17] G. Mena, D. Belanger, S. Linderman, and J. Snoek. Learning latent permutations with gumbel-sinkhorn networks. *arXiv preprint arXiv:1802.08665*, 2018. [4](#)
- [18] A. Mousavian and J. Kosecka. Semantic image based geolocation given a map. *arXiv preprint arXiv:1609.00278*, 2016. [2](#)
- [19] D. Nister and H. Stewenius. Scalable recognition with a vocabulary tree. In *2006 IEEE Computer Society Conference on Computer Vision and Pattern Recognition (CVPR'06)*, volume 2, pages 2161–2168. Ieee, 2006. [2](#)
- [20] O. Russakovsky, J. Deng, H. Su, J. Krause, S. Satheesh, S. Ma, Z. Huang, A. Karpathy, A. Khosla, M. Bernstein, et al. Imagenet large scale visual recognition challenge. *International Journal of Computer Vision*, 115(3):211–252, 2015. [2](#)
- [21] R. Santa Cruz, B. Fernando, A. Cherian, and S. Gould. Deep-permnet: Visual permutation learning. In *Proceedings of the IEEE Conference on Computer Vision and Pattern Recognition*, pages 3949–3957, 2017. [4](#)
- [22] K. Simonyan and A. Zisserman. Very deep convolutional networks for large-scale image recognition. *arXiv preprint arXiv:1409.1556*, 2014. [4](#)
- [23] J. Sivic and A. Zisserman. Video google: A text retrieval approach to object matching in videos. In *null*, page 1470. IEEE, 2003. [2](#)
- [24] J. Sivic and A. Zisserman. Video google: Efficient visual search of videos. In *Toward category-level object recognition*, pages 127–144. Springer, 2006. [2](#)
- [25] N. N. Vo and J. Hays. Localizing and orienting street views using overhead imagery. In *European Conference on Computer Vision*, pages 494–509. Springer, 2016. [3](#), [5](#), [6](#), [7](#)
- [26] S. Workman and N. Jacobs. On the location dependence of convolutional neural network features. In *Proceedings of the IEEE Conference on Computer Vision and Pattern Recognition Workshops*, pages 70–78, 2015. [2](#), [3](#)
- [27] S. Workman, R. Souvenir, and N. Jacobs. Wide-area image geolocalization with aerial reference imagery. In *Proceedings of the IEEE International Conference on Computer Vision*, pages 3961–3969, 2015. [3](#), [7](#)
- [28] M. D. Zeiler and R. Fergus. Visualizing and understanding convolutional networks. In *European conference on computer vision*, pages 818–833. Springer, 2014. [1](#)
- [29] M. Zhai, Z. Bessinger, S. Workman, and N. Jacobs. Predicting ground-level scene layout from aerial imagery. In *IEEE Conference on Computer Vision and Pattern Recognition*, volume 3, 2017. [2](#), [5](#), [7](#), [8](#), [10](#)
- [30] B. Zhou, A. Lapedriza, J. Xiao, A. Torralba, and A. Oliva. Learning deep features for scene recognition using places database. In *Advances in neural information processing systems*, pages 487–495, 2014. [2](#)

Appendices

A. Visualization of cross-view feature map alignment

Additional examples of cross-view feature maps before and after our cross-view feature transport (CVFT) module are presented in Figure 11. It demonstrates that the proposed CVFT is able to align the feature maps of the cross-view images effectively.

B. The impact of dimensionality reduction

The dimension of our feature embedding is 4096, which is as the same as that of CVM-net [7]. In Liu *et al.*'s work [14], the dimension is 1536. To illustrate the impact of feature embedding dimensions on cross-view localization performance, we resize the output feature map to different spatial sizes, thus leading to different feature embedding dimensions. The recall performance of the proposed CVFT in different feature embedding dimensions on CVUSA [29] and CVACT [14] datasets is given in Table 4. It shows that our recall performance decreases gradually with the decrease of feature embedding dimension, yet still outperforms state-of-the-art methods [7, 14].

C. Visualization of cross-view embeddings

The goal of our method is to embed cross-view image features under a same space, where cross-view features of the same scene lie close to each other. To verify it, we adopt t-SNE [16] to visualize the cross-view embeddings of CVACT [14] dataset by our method. The results as seen in Figure 12 illustrate that the matched cross-view image pairs are embedded into nearby positions in the embedding space despite significant view point changes.

Table 4: Recall performance of our CVFT under different feature embedding dimensions

Dataset \ Dimensionality	CVUSA				CVACT_val			
	r@1	r@5	r@10	r@top 1%	r@1	r@5	r@10	r@top 1%
4096	61.43	84.69	90.49	99.02	61.05	81.34	86.52	95.93
2048	56.43	80.77	88.07	98.81	57.86	79.69	85.25	95.49
1536	52.22	77.30	85.31	98.33	53.94	77.40	83.27	95.09
512	43.05	69.42	78.66	96.89	44.69	70.19	77.81	93.56
4096 (CVM-net [7])	22.47	49.98	63.18	93.62	17.53	42.13	53.15	86.72
1536 (Liu etal [14])	40.79	66.82	76.36	96.12	46.96	68.28	75.48	92.04

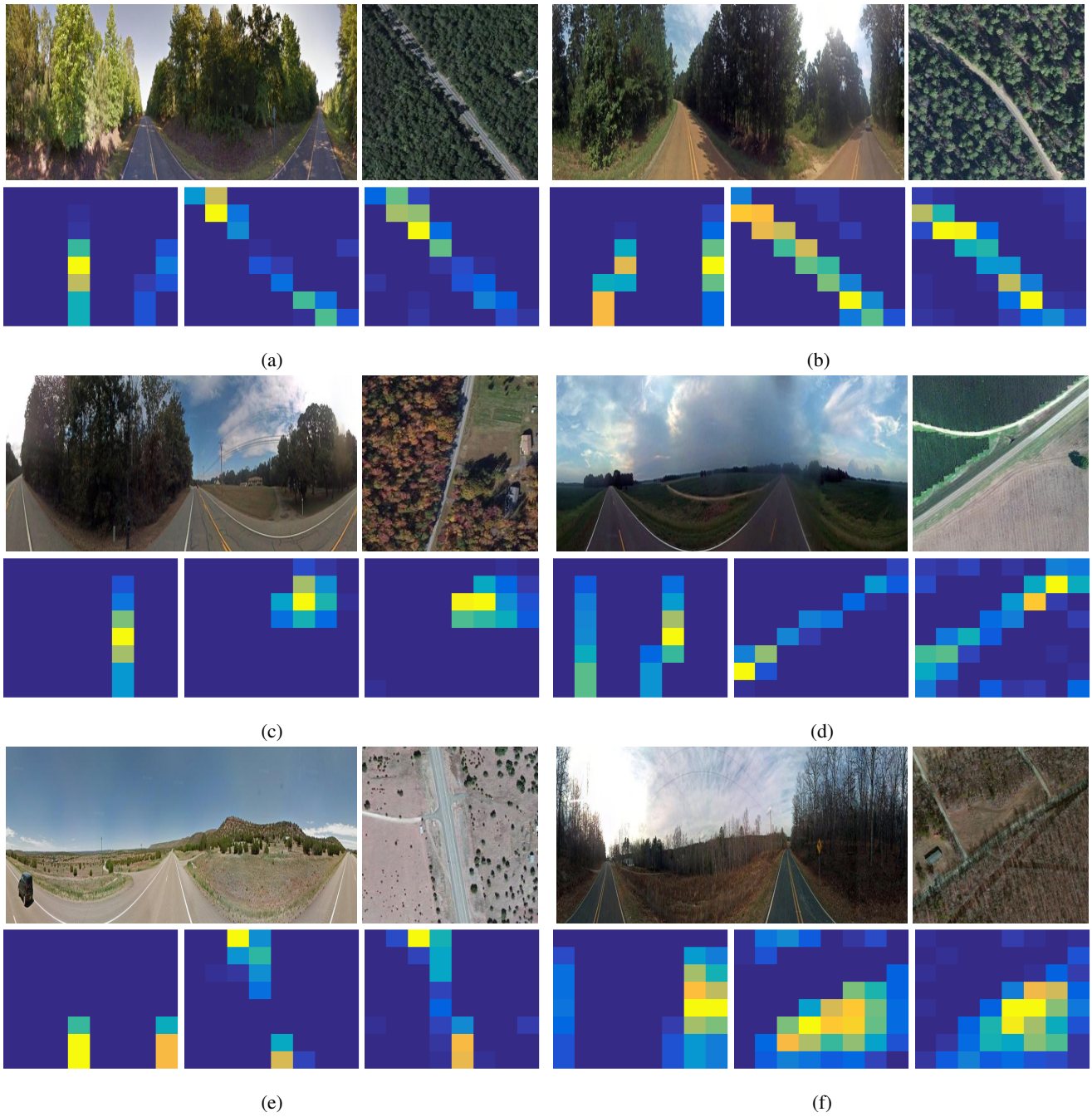


Figure 11: Additional examples for demonstrating the effectiveness of the proposed CVFT on aligning cross-view feature maps. In each of the second rows, (Left column:) Input ground-view feature map; (Middle column) the corresponding satellite image feature map; (Right column) CVFT-transported ground-view feature map. Note the CVFT-transported ground-view feature map and original satellite image feature map are well-aligned.

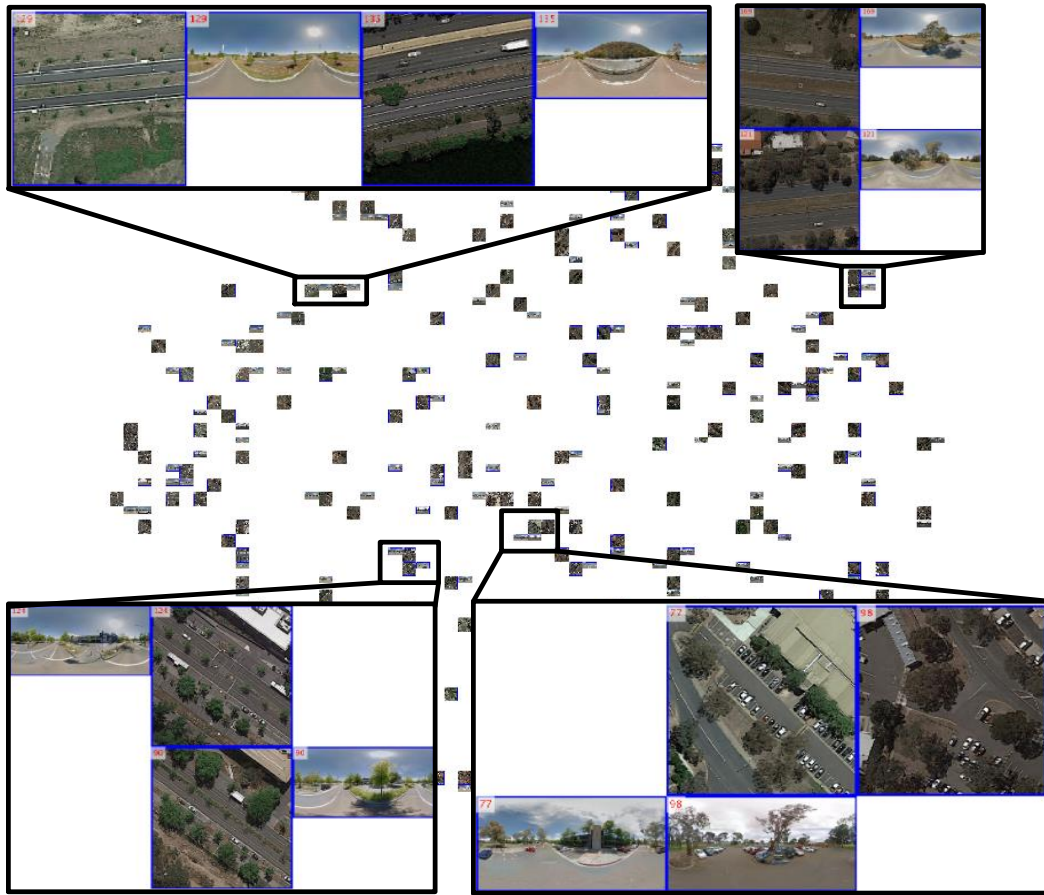


Figure 12: Visualization of cross-view feature embeddings using t-SNE [16] on CVACT [14] dataset. The red number on the left-top corner of each image is the ID of a cross-view image pair. (Best viewed on screen with zoom-in)